31st Annual International Conference of the IEEE EMBS
Minneapolis, Minnesota, USA, September 2-6, 2009

MRI-compatible Micromanipulator: Positioning Repeatability Tests & Kinematic Calibration

Yoshihiko KOSEKI, Tamio TANIKAWA, and Kiyoyuki CHINZEI

Abstract— **In this paper, we report results from positioning repeatability tests and kinematic calibration of our magnetic resonance imaging (MRI)-compatible micromanipulator. This manipulator provides medical and biological scientists with the ability to concurrently manipulate and observe micrometer size objects inside an MRI-gantry. We have already reported on its design, implementation, and the results of preliminary testing of MRI compatibility. Here we test positioning repeatability, which is essential for micromanipulation. The results show that the manipulator has high repeatability (0.7 μm in longitude and 3.0 μm in latitude). In addition, we performed a calibration of kinematics and discussed the experimental result in comparison with the theoretical model. The results show that its workspace is 50–70% smaller than theoretically expected. The results also show that the absolute positioning errors are 16, 9, 5 μm in x, y, and z directions, respectively.**

I. INTRODUCTION

The capability of operation and observation on microscale structure and behavior of living tissues and cells is increasingly in demand in biology and medical science. Magnetic resonance imaging (MRI) has evolved into a powerful tool for observing living molecules non-invasively. In addition, advanced micromanipulators that can operate on microscale objects have been developed.

An MRI device detects a weak radio wave excited by a strong radio wave in a strong and precise magnetic field. Because the radio wave is unique to a molecule and its position, the MRI can generate a map of the molecules in a system. Using an MRI, the operator can visualize the distribution of a molecule as well as cells and proteins labeled by contrast agents. An MRI device therefore enables medical, biological, and psychological scientists to observe not only the shape but also the tissue activity of patients and animals [1].

Medical and biological scientists often need to move, hold, cut, and sting microscopic biological cells and tissues. Researchers have studied mechanical and mechatronical systems designed to provide the dexterous micron-scale manipulation capability needed to satisfy these requirements [2].

We have studied an MRI-compatible micromanipulator that can provide medical and biological scientists with microscale manipulation inside an MRI gantry [3]. The potential merits of this device are that the MRI enables visualization of an object's response to mechanical changes on-site, whereas the micromanipulator operates on the object based on real time, on-site information obtained from the MRI. Such technique allows for non-conventional interactive experiments on living tissue and can save significant time for medical and biological scientists.

We have already reported on the manipulator's design, implementation, and MRI-compatibility validation [3]. The results of that study revealed that the operation of the manipulator produced some electrical noise in the MRI signal. Although these results suggested that improvements are necessary with respect to electromagnetic compatibility, it was, nevertheless, possible to obtain an MRI signal while the manipulator was inside the MRI-gantry.

In this paper, we examine the accuracy of an MRI-compatible micromanipulator outside an MRI-gantry. We first validate positioning repeatability, which is essential for effective micromanipulation. Then, we calibrate the kinematics of the micromanipulator and discuss the results in comparison with a theoretical model. Finally, we evaluate absolute positioning accuracy after the calibration.

II. MATERIALS & METHODS

A. MRI-compatible Micromanipulator

Figure 1 shows the mechanical system of the micromanipulator. The micromanipulator controls two finely tapered glass needles and forms a two-finger micro-hand, as studied in [2]. The lower endplate moves both the lower needle and the upper endplate and produces absolute motion corresponding to the thumb. The upper endplate moves the upper needle and produces relative motion to the lower needle corresponding to the index finger. Screws are used to adjust the initial relative position of the lower needle with respect to that of the upper needle.

Figure 2 is a schematic that shows the mechanism, coordinate system, and dimensions of the micromanipulator. Both needles are moved by parallel mechanisms with three degrees of freedom. The lower endplate is supported by three linear actuators (Axis 1–3) in parallel. When all of the actuators are extended, the endplate exhibits translational motion along the longitude (z^m). When only one actuator (e.g., Axis 2) is extended, the endplate slightly inclines and exhibits approximately translational motion in the latitude direction (y^m). The same mechanism is used in the upper endplate. The lever amplification mechanisms are implemented with actuators (see Fig. 3).

Yoshihiko KOSEKI is with the National Institute of Advanced Industrial Science and Technology (AIST), 1-2-1 Namiki, Tsukuba, Ibaraki 305-8564, Japan

Tamio TANIKAWA is with the National Institute of Advanced Industrial Science and Technology (AIST), 1-1-1 Umezono, Tsukuba, Ibaraki 305-8568, Japan

Kiyoyuki CHINZEI is with the National Institute of Advanced Industrial Science and Technology (AIST), 1-2-1 Namiki, Tsukuba, Ibaraki 305-8564, Japan

978-1-4244-3296-7/09/$25.00 ©2009 IEEE

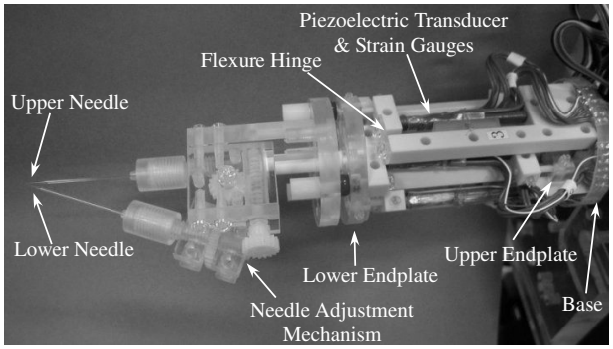

Fig. 1. Prototype of MRI-compatible Micromanipulator

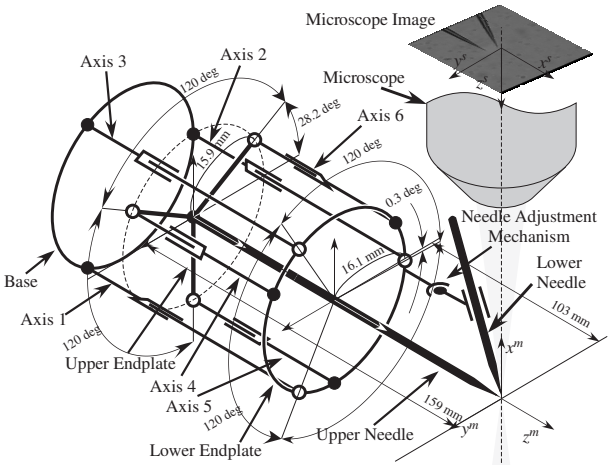

Fig. 2. Coordinate system definition and dimensions of micromanipulator and mesurement system

The materials used for this mechanism are mainly acrylic plastic and machinable ceramics in addition to some polyacetal resin. All of the hinge joints in the mechanism function as flexure hinges.

The linear actuators are resin-coated multilayer piezoelectric transducers (AE0203E44H40, NEC-Tokin), because micron-scale linear motion is required and these devices are non-magnetic. Their stroke is 42.0 μm at the maximum applied voltage of 150 V. The relationship between the stroke (l) and the applied voltage (v) is approximated as follows.

$$l = \frac{42}{150}\, v \tag{1}$$

Because of the hysteresis inherent in piezoelectric transducers, it is difficult to control the extension precisely using applied voltage. Therefore, strain (which is proportional to the extension) is measured using a strain gauge, and the applied voltage is controlled with a proportional-derivative feedback so that the strain output equals the set value. The gain and offset of the strain amplifier are adjusted to maintain its output range (1.0–10 V) with the margin of offset drift (0.5 V) while 0–150 V is applied to the transducer. Finally, the applied voltage to the output of the strain amplifier (u) is approximated as follows.

$$v = \frac{150}{10}\,(1.15u - 1.92) \tag{2}$$

The analog output of the strain amplifier is converted to a digital signal ($\pm$10V 12bit analog-to-digital converter), and the converted value is defined as a command (d). Because this system operates on single power supplies, the value of the command could range from 2047 to 4095.

$$u = 10\frac{d - 2047.5}{2047.5} \tag{3}$$

B. Position Measuring Instrument

The position measurements done for repeatability tests and calibration were carried out using microscopic images. A microscope (BH2, Olympus Co., Ltd.) was used to view the tips of the needles, and the images were captured by a CCD camera (DXC-C33, SONY Co.) and stored in a computer (IEEE1394 based). The effective image size was 704 $\times$ 480 pixels. The positions of the needle tips were judged by the microscope operator. The microscope was equipped with low- and high-power objective lenses (IC5 and IC20, respectively) and a projector lens (NFK5).

Optical distortion and pixel size of the microscopic system were tested using a precision test target (CA002E, Edmund optics) that featured equally spaced vacuum-deposited straight lines (10 lines per millimeter). The results showed that the optical distortion was sufficiently small and that straightness was maintained in the captured images. The pixel sizes were 0.88 $\times$ 0.97 μm and 0.22 $\times$ 0.24 μm, respectively, for the low- and high-power lenses.

The displacement in depth (z^s in Fig. 2) was measured by changing the focus of the microscope. A microstage, on which the micromanipulator was mounted, moved along the optic axis to the position where the tip of needle was well focused. The displacement of the microstage in depth was measured by a digital linear gauge (DG525, ONO SOKKI Tech. Inc.). Because focusing was judged by the microscope operator, the error in position measurement was large relative to that for the microscopic image.

C. Positioning Repeatability Tests

Since the micromanipulator is a cylindrical structure, the positioning errors in the two latitudinal directions (x^m and y^m) were assumed to be equal. Accordingly, the micromanipulator was oriented to put z^m and x^s, y^m and y^s, and x^m and z^s in parallel. The tip of the needle was viewed with the high-power objective lens (IC20).

The micromanipulator positioned the needle at a measurement point and the tip of needle was focused. The needle was next moved randomly away from the measurement point and then moved back to it where the final position of the needle tip was measured. These procedures were repeated 30 times for each measurement point.

Initially, position measurement was done when the positioning control was disabled (1 point). The commands for upper endplate were fixed to its home position ($\vec{d_1} = (3071, 3071, 3071)$), and those for lower endplate were switched $\pm$25% ($\vec{d_2} = (3071\pm512, 3071\pm512, 3071\pm512)$) ($2 \times 2 \times 2 = 8$ points). In the same way, the commands for the lower endplate were fixed to its home position ($\vec{d_2} =$

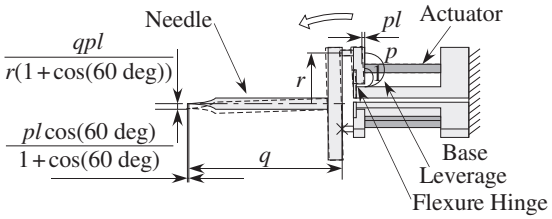

Fig. 3. Forward kinematics model

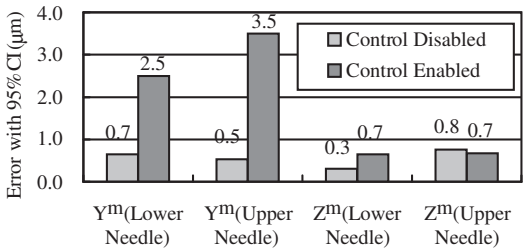

Fig. 4. Repeatability of micromanipulator at 95%CI, latitudinal(y) and longitudinal(z) axes, control activated and deactivated, upper and lower needle.

$(3071, 3071, 3071)$), and those for the upper endplate were switched ($2 \times 2 \times 2 = 8$ points). The commands for both the upper and lower endplates were fixed to their home positions (1 point). For those points, upper and lower needles were subject to position measurements. In total, there measured at 30 times in 36 conditions.

D. Kinematic Calibration

The kinematics of the micromanipulator can be approximated linearly since the displacements involved are small. Relationships between the extensions of the piezoelectric actuators and the displacements of needles are formulated as the following linear matrix equation. The quantities $\vec{x}_1$, $\vec{x}_2 \in 3 \times 1$ are the displacements of lower needle and upper needle, respectively, and $\vec{l}_1$, $\vec{l}_2 \in 3 \times 1$ are extensions of lower and upper actuators, respectively. The expression for $F_{11} \cdots F_{22} \in 3 \times 3$ is as follows:

$$\left(\frac{\vec{x}_1^m}{\vec{x}_2^m}\right) = \left(\frac{F_{11} \mid F_{12}}{F_{21} \mid F_{22}}\right) \left(\frac{\vec{l}_1}{\vec{l}_2}\right) \tag{4}$$

The displacements of the needle are modeled as shown in Fig. 3. The parameter p is a ratio of lever amplification mechanisms, q is a length of needle, r is the radius of a circle including all points of application. It is assumed that the extension of an actuator is proportional to the corresponding command. The following equations were obtained from this model, with $r = 2.0$, and the parameters shown in Fig. 2, and (1)–(3). The commands for actuators acting on the lower and upper endplates are given by $\vec{d}_1$, $\vec{d}_2 \in 3 \times 1$, respectively.

$$\left(\frac{\vec{x}_1^m}{\vec{x}_2^m}\right) = \left(\frac{G_{11} \mid G_{12}}{G_{21} \mid G_{22}}\right) \left(\frac{\vec{d}_1}{\vec{d}_2}\right) \tag{5}$$

$$G_{11} = \begin{pmatrix} 0.1736 & 0.0009 & -0.1745 \\ -0.1013 & 0.2010 & -0.0997 \\ 0.0157 & 0.0157 & 0.0157 \end{pmatrix} \tag{6}$$

$$G_{12} = \begin{pmatrix} 0.0 & 0.0 & 0.0 \\ 0.0 & 0.0 & 0.0 \\ 0.0 & 0.0 & 0.0 \end{pmatrix} \tag{7}$$

$$G_{21} = G_{11} \tag{8}$$

$$G_{22} = \begin{pmatrix} 0.1660 & -0.3148 & 0.1488 \\ 0.2677 & 0.0099 & -0.2775 \\ -0.0157 & -0.0157 & -0.0157 \end{pmatrix} \tag{9}$$

The calibration process was used to obtain $G_{11} \cdots G_{22} \in 3 \times 3$. Random commands were input initially, and the 3-dimensional displacements of the needles were measured and transformed into the micromanipulator's coordinate system. Equation (10) was then used with these commands and positions of the measurement points, and $G_{11} \cdots G_{22}$ was numerically obtained by minimizing the sum of squares errors. A total of 50 points were measured for calibration, and another 50 points were used for absolute positioning error tests. These measurements were performed alternately.

$$\sum_{i=1}^{n} \left(\frac{\vec{e}_1}{\vec{e}_2}\right)^T \left(\frac{\vec{e}_1}{\vec{e}_2}\right) \rightarrow min \tag{10}$$

Noting that

$$\left(\frac{\vec{e}_1}{\vec{e}_2}\right) = \left(\frac{\vec{x}_1^m}{\vec{x}_2^m}\right) - \left(\frac{G_{11} \mid G_{12}}{G_{21} \mid G_{22}}\right) \left(\frac{\vec{d}_1}{\vec{d}_2}\right) \tag{11}$$

III. RESULTS & DISCUSSIONS

A. Positioning Repeatability Tests

Figure 4 shows the level of repeatability (at a 95% Confidence Interval (CI)) of the latitudinal (y-axial) and longitudinal (z-axial) lower and upper needle positioning when the control is disabled compared to when it is enabled. Averaged results are displayed in this figure.

The latitudinal positioning error is much larger than the longitudinal. This difference is expected, because the latitudinal workspace is much larger than the longitudinal workspace. The error of the upper needle is larger than that of the lower needle. This difference was also anticipated, because the upper endplate is mounted on the lower endplate, which means that the lower and upper endplates are both involved in positioning the upper needle. Even when the control was disabled, the positioning error was not zero. It is likely that this error includes a measurement error and the effects of noise caused by environmental factors (e.g., floor vibration and temperature fluctuations).

B. Kinematic Calibration

Equations (12)–(15) are the matrices of linear kinematics obtained experimentally.

$$G_{11} = \begin{pmatrix} 0.0827 & 0.0104 & -0.0904 \\ -0.0651 & 0.1104 & -0.0209 \\ 0.0093 & 0.0115 & 0.0093 \end{pmatrix} \tag{12}$$

$$G_{12} = \begin{pmatrix} 0.0010 & 0.0039 & -0.0033 \\ -0.0093 & 0.0001 & 0.0026 \\ 0.0008 & 0.0005 & 0.0003 \end{pmatrix} \tag{13}$$

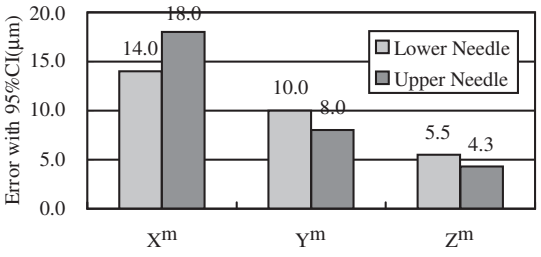

Fig. 5. Absolute positioning error after calibration

$$G_{21} = \begin{pmatrix} 0.0791 & 0.0166 & -0.0908 \\ -0.0689 & 0.1024 & -0.0124 \\ 0.0084 & 0.0109 & 0.0089 \end{pmatrix} \quad (14)$$

$$G_{22} = \begin{pmatrix} 0.0883 & -0.1489 & 0.0653 \\ 0.1359 & 0.0118 & -0.1346 \\ -0.0081 & -0.0087 & -0.0086 \end{pmatrix} \quad (15)$$

These matrices are 50–70% smaller than theoretical ones. An additional experiment revealed that the amplification of the actuator was less than what was theoretically expected. This result might be caused by hinge flexure, which is not accounted for in the model. For a conventional flexure mechanism, a flexure hinge works as an ideal revolute joint, because it is made from a single piece of metal precisely machined using an electrical discharge machining process. Therefore, a kinematic model can be constructed assuming a perfect joint and rigid body motion that correlates with actual kinematics. In lieu of using a sophisticated computational algorithm (such as the finite element method), this model is useful for the design of both the kinematics and workspace [4]. For the MRI-compatible manipulator, the flexure element is made of acrylic plastic and the rigid part is constructed of machinable ceramics (to ensure electromagnetic compatibility with the MRI system). As a result, unexpected translational displacement could occur at the boundary between the flexure joint and the rigid part.

Figure 5 shows the absolute positioning error of the upper and lower needles after calibration at a 95% CI. This error may be mainly due to the position measuring in depth. The difference between y and z could be caused by the difference of workspace size.

IV. CONCLUSIONS AND FUTURE WORK

In this paper, we report positioning repeatability tests and kinematic calibration of our MRI-compatible micromanipulator outside of the MRI-gantry. The repeatability tests revealed that the manipulator has, on average, a 0.7 μm longitudinal error and a 3.0 μm latitudinal error at a 95% CI. This accuracy is sufficient for manipulation of blood capillary and nerve fiber. Even when the control was disabled, the needles positioned with significant error (0.5 μm both longitudinally and latitudinally) Such errors could be the result of the noise associated with environmental factors such as floor vibrations and temperature fluctuations. In an environment of conventional micromanipulation, vibration isolation and precise temperature control can be expected. However, these factors are generally not controlled in an MRI environment. We also note that optimal component design and careful material selection are necessary for ensuring vibration isolation and reducing the effects of thermally driven deformation.

We also carried out a kinematic calibration and discussed the experimental results we obtained compared to a theoretical model. The calibration revealed that the kinematics matrices were 50–70% smaller than the theoretical matrices. This difference suggests that the workspace is smaller than theoretically expected. We suspect that the underlying cause of such discrepancies is related to the flexure hinge in the micromanipulator that does not function as an ideal revolute joint. It is likely that some improvements in the design and fabrication of the flexure hinges are required. An absolute positioning accuracy was determined after calibration. The results of this determination suggest that the absolute positioning errors are 16, 9, and 5 μm in x, y, and z directions, respectively. This error can be larger than the actual absolute positioning error of the manipulator due to problems of position measurement in depth; however, these results confirm that the absolute accuracy of this manipulator is adequate for the intended application of MRI-compatible micromanipulator.

V. ACKNOWLEDGMENTS

This research was partially funded by Grants-in-Aid for Young Scientists (#B17700419) from the Japan Society for the Promotion of Science (JSPS) and Research and Development of Three-dimensional Complex Organ Structures (Project ID: P06043) from New Energy and Industrial Technology Development Organization (NEDO).

REFERENCES

[1] L. Ciobanu, et al.: "Magnetic resonance imaging of biological cells", Progress in Nuclear magnetic Resonance Spectroscopy, Vol. 42, 2003, pp. 69-93

[2] T. Tanikawa, T. Arai, N. Koyachi: "Development of Small-sized 3 DOF Finger Module in Micro Hand for Micro Manipulation", Proc. IEEE/RSJ IROS 1999, pp. 876-881, 1999

[3] Y. Koseki, T.Tanikawa, K. Chinzei: "MRI-compatible Micromanipulator, Design and Implementation and MRI-compatibility Tests", Proc. of EMBC 2007, pp. 465-468, 2007

[4] Y. Koseki, T. Tanikawa, N. Koyachi, T. Arai: "Kinematic analysis of a translational 3-d.o.f. micro-parallel mechanism using the matrix method", Robotics Society of Japan Advanced Robotics, Vol.16, No.3, pp. 251-264, 2002